SUPPLEMENTAL MATERIALS

High salt intake worsens aortic dissection in mice: involvement of IL-17A-dependent extracellular matrix metabolism

Norifumi Nishida, MD [1], Hiroki Aoki, MD, PhD [2], Satoko Ohno-Urabe, MD, PhD [1], Michihide Nishihara, MD, PhD [1], Aya Furusho, MD, PhD [1], Saki Hirakata, MD [1], Makiko Hayashi, MD [1], Sohei Ito, MD [1], Hiroshi Yamada, PhD [3], Yuichiro Hirata, MD, PhD [4], Hideo Yasukawa, MD, PhD [1], Tsutomu Imaizumi, MD, PhD [5], Hiroyuki Tanaka, MD, PhD [4], Yoshihiro Fukumoto, MD, PhD [1]

Affiliations

1. Division of Cardiovascular Medicine, Department of Internal Medicine, Kurume University School of Medicine, Kurume, Japan
2. Cardiovascular Research Institute, Kurume University, Kurume, Japan
3. Department of Biological Functions Engineering, Graduate School of Life Science and Systems Engineering, Kyushu Institute of Technology, Kitakyushu, Japan
4. Division of Cardiovascular Surgery, Department of Surgery, Kurume University School of Medicine, Kurume, Japan
5. International University of Health and Welfare, Fukuoka, Japan

Major Resources Tables

Animals (in vivo studies)

Species	Vendor or Source	Background Strain	Sex
Mouse	Tokyo University of Science, Center for Animal Disease Models	C57BL/6J	Male

Animal breeding

	Species	Vendor or Source	Background Strain	Other Information
Parent - Male	Mouse	Tokyo University of Science, Center for Animal Disease Models	C57BL/6J	*Il17a* deleted
Parent - Female	Mouse	Tokyo University of Science, Center for Animal Disease Models	C57BL/6J	*Il17a* deleted

Antibodies

Target antigen	Vendor	Catalog #	Working concentration (μg/mL)	Applications
β-actin	Cell Signaling Technology (CST)	#4970	0.05	WB
Calponin 1	Abcam	#ab46794	0.02	WB
GAPDH	Millipore	#MAB374	0.2	WB
NFkB	CST	#8242	1	WB
P-Jnk	CST	#4671	0.9	WB
P-NFkB	Enogene	#E011260-1	1	WB
P-Smad2	CST	#3108	0.05	WB

Antibodies (cont'd)

Target antigen	Vendor	Catalog #	Working concentration (μg/mL)	Applications
P-Smad3	Abcam	#ab52903	0.25	WB
P-Stat3	CST	#9145	0.5	WB
SM2	Yamasa	#7601	1:400, ascites (antibody concentration undetermined)	WB
Smad2	CST	#5339	0.28	WB
Smad3	Abcam	#ab40854	1	WB
Smad4	Abcam	#ab195554	0.1	WB
Smad7	Abcam	#ab190987	0.5	WB
SMemb	Abcam	#ab684	1:1000, ascites (antibody concentration undetermined)	WB
Vimentin	Abcam	#ab92547	0.25	WB
Mouse IgG	Jackson ImmunoResearch	#715-165-151	7.5	IF, Cy3-conjugated donkey anti-mouse IgG antibody
pSmad2	ThermoFisher	#44-244G	2.0	IF
Rabbit IgG isotype control	Abcam	#ab172730	2.0	IF
Smooth muscle α-actin	Sigma-Aldrich	#A5228	0.2	IF
Mouse IgG2a isotype control	Sigma-Aldrich	#MABC004	0.2	IF

Cultured Cells

Name	Vendor or Source	Sex
Aortic smooth muscle cells, #JCRB0150	The National Institutes of Biomedical Innovation, Health and Nutrition (Tokyo, Japan)	Unknown

SUPPLEMENTAL FIGURES

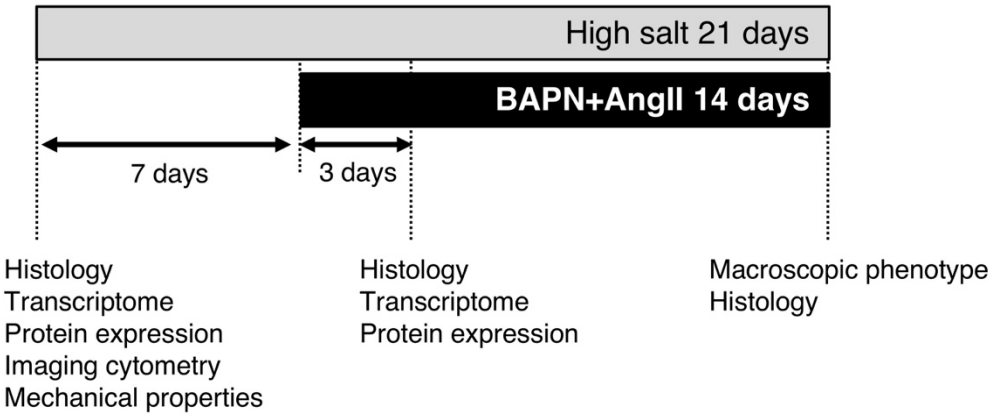

Supplemental Figure SI. Protocol for animal experiments.

The diagram shows the protocol for animal experiments. High salt condition (1% NaCl in drinking water) was maintained for 7 days before and throughout the AD-induction period with BAPN+AngII. Histological and expression analyses were performed 3 days after starting BAPN+AngII when visible AD was not observed. Macroscopic phenotype and histological analyses were performed at the end of 14 days of BAPN+AngII with or without high salt challenge.

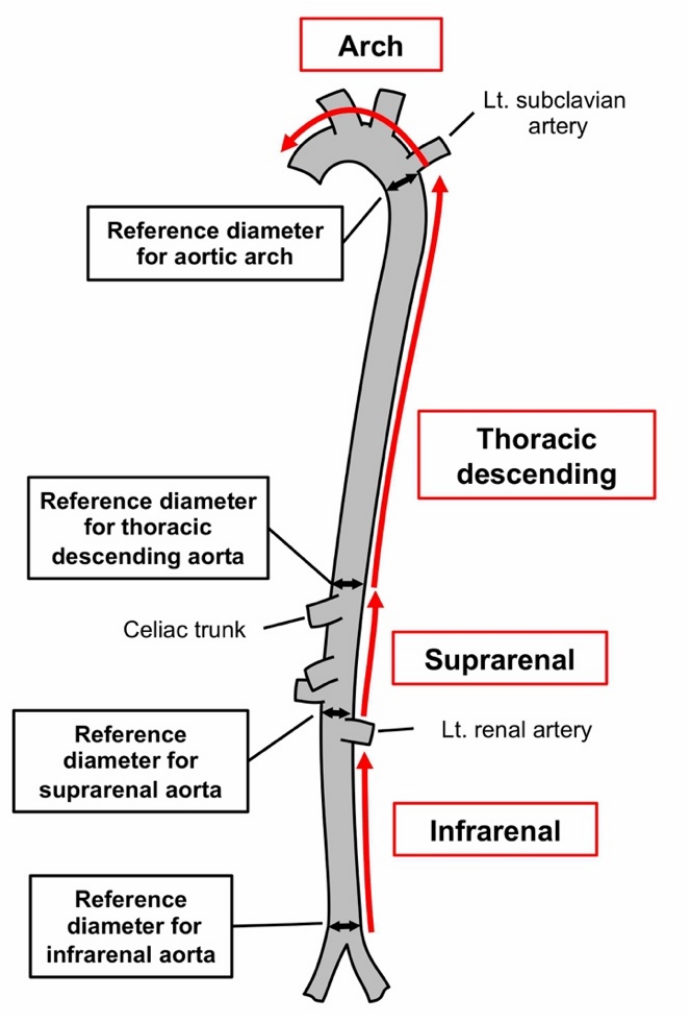

Supplemental Figure SII. Regional assessment of aortic wall destruction in the AD model.

The diagram shows the aortic segments (red arrows) and corresponding reference diameters at the distal site of each segment (black double arrows). The lesion length with aortic wall destruction due to AD was measured in four segments: the arch, thoracic descending, suprarenal, and infrarenal. In this study, a lesion with aortic wall destruction due to AD was defined by an at least 1.5-fold increased diameter compared to the reference diameter in each segment. The reference diameters were measured in eight mice of the relevant genotype and the mean values used.

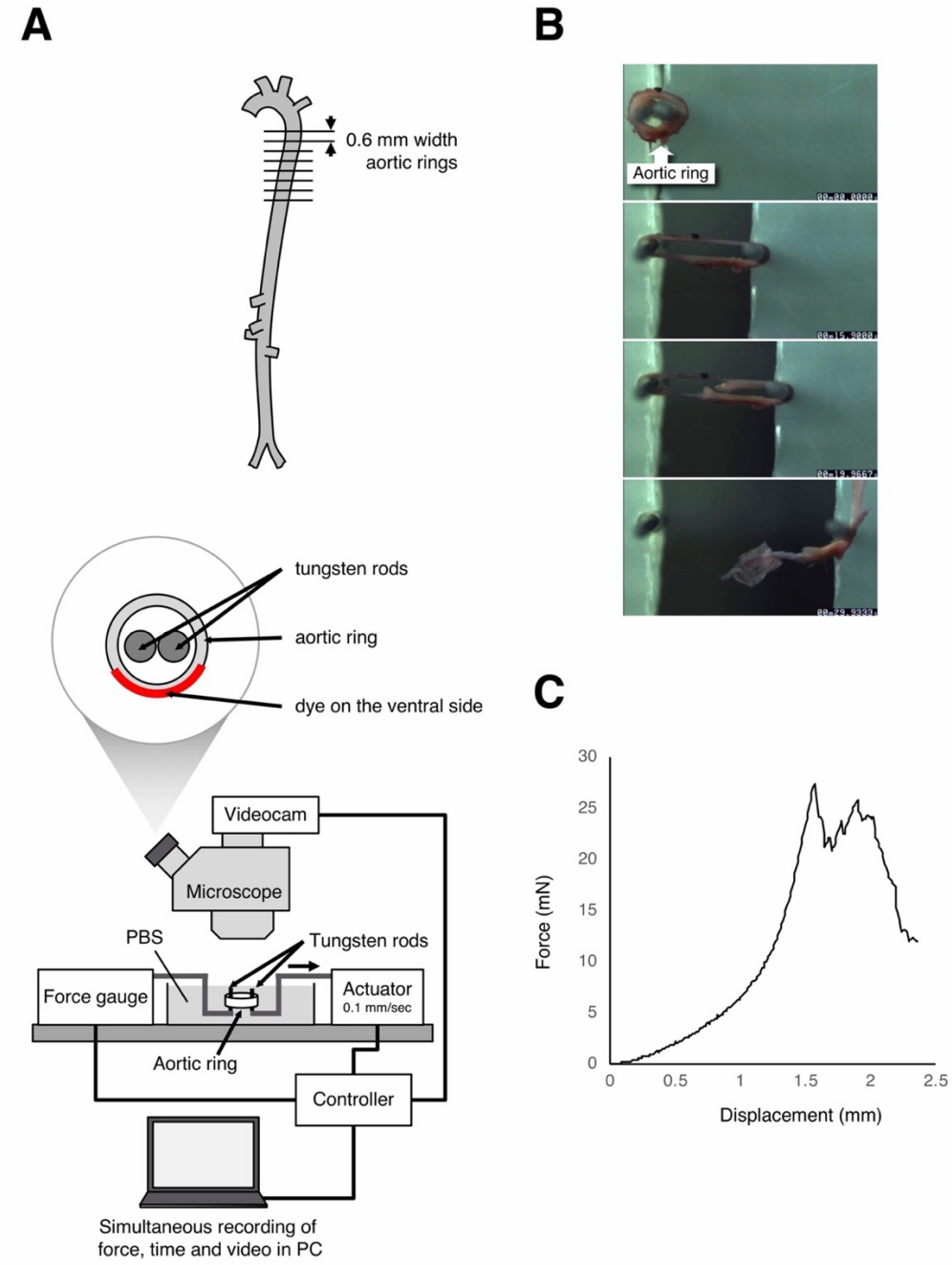

Supplemental Figure SIII. Measurement of the biomechanical properties of the aortic wall.

(A) Diagrams of the procurement of aortic rings from the descending thoracic aorta (top) and the device for measuring the force-displacement relationship of the aortic rings (bottom). (B, C) A representative video recording (B) and force-displacement curve (C).

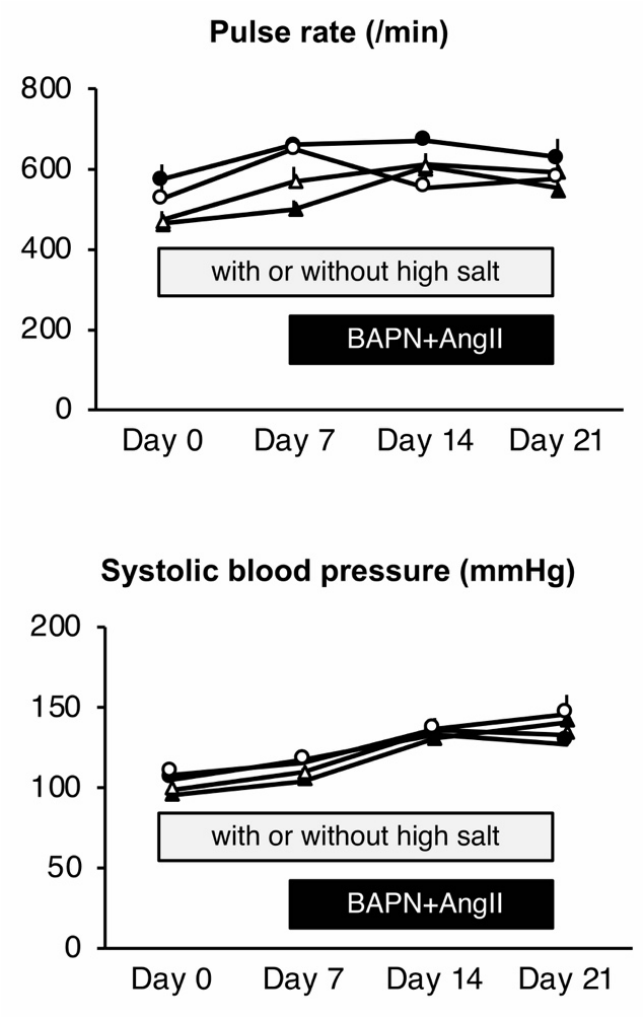

Supplemental Figure SIV. Hemodynamic parameters in the AD model.

Pulse rate and systolic blood pressure in the AD model with (High salt, closed symbols) or without high salt (Normal salt, open symbols) intake in wild-type (circles) and IL-17KO (triangles) mice. Data represent the mean ± standard error for 8–12 mice in each group.

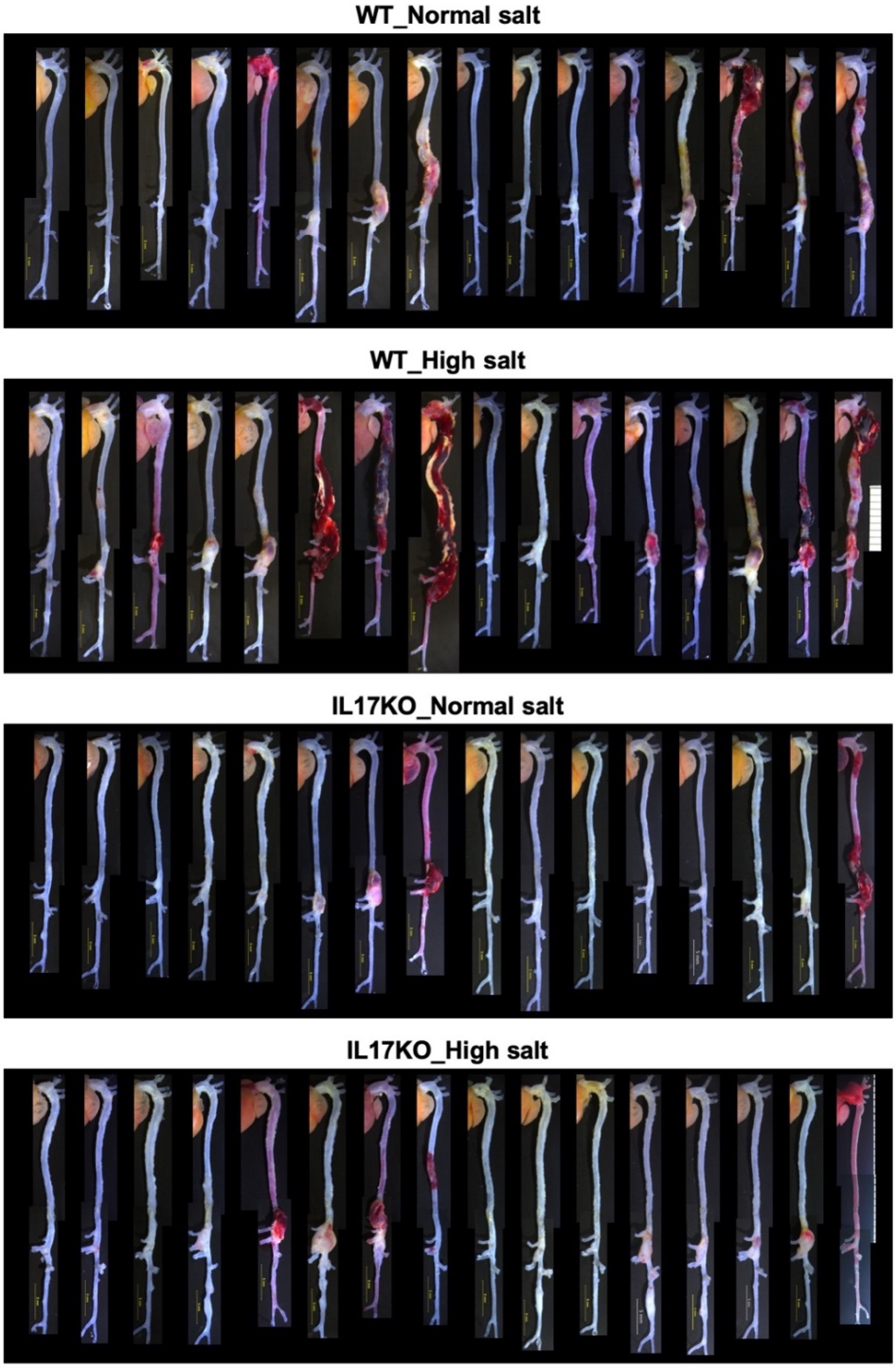

Supplemental Figure SV. Macroscopic images of mouse AD model. Macroscopic images are shown for aortas of wild type (WT) and IL-17KO mice 14 days after starting BAPN+AngII infusion with (High salt) and without (Normal salt) high salt challenge.

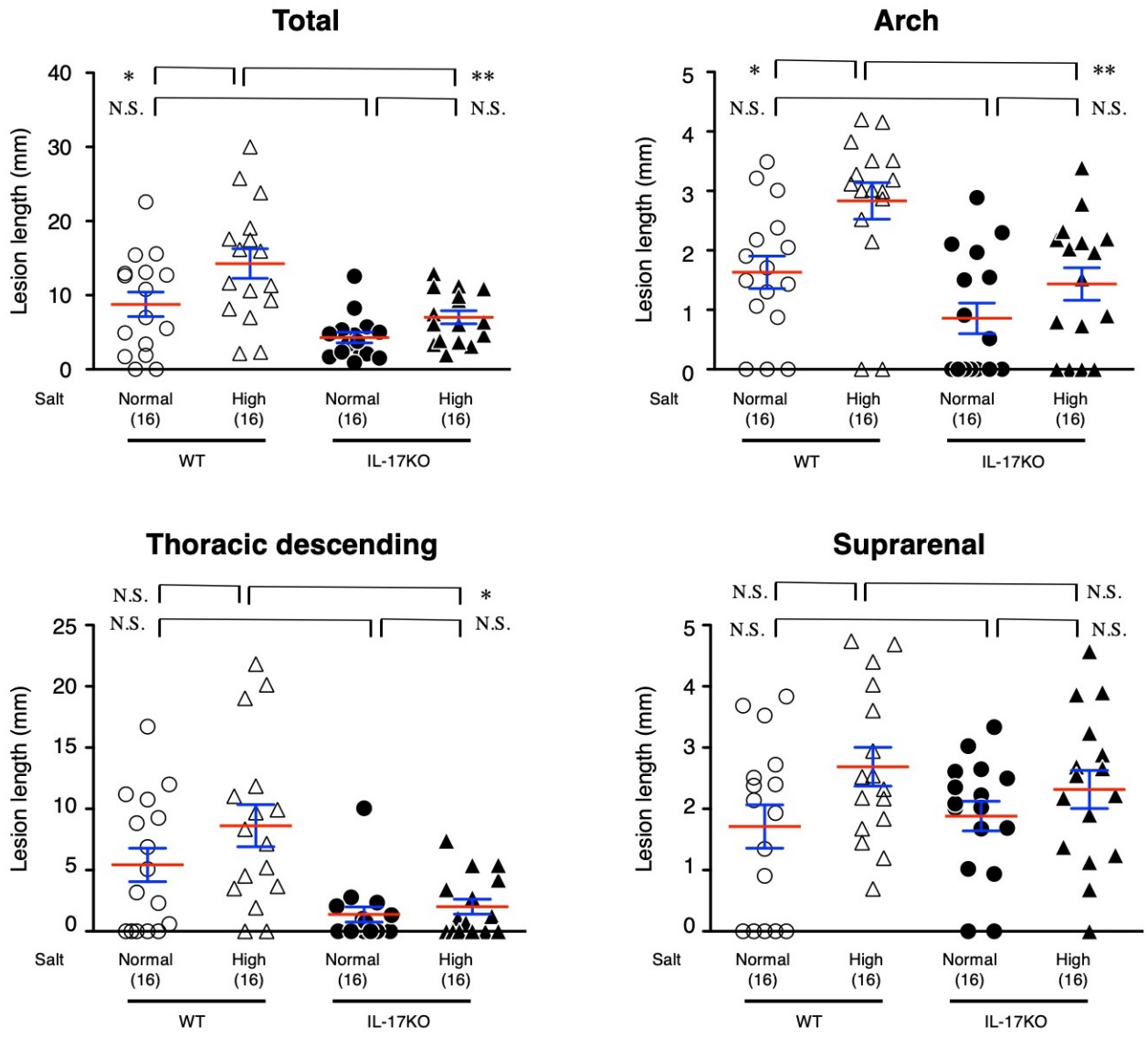

Supplemental Figure SVI. AD lesion length in each aortic segment and lesion scores.

The AD lesion lengths are shown for individual aortic segments. The data were obtained from the same set of experiments as shown in Figure 2B. Data are presented as the mean (red lines) ± standard error (blue lines) of 16 mice in each experimental group; N.S., not significant, * $p < 0.05$, ** $p < 0.01$.

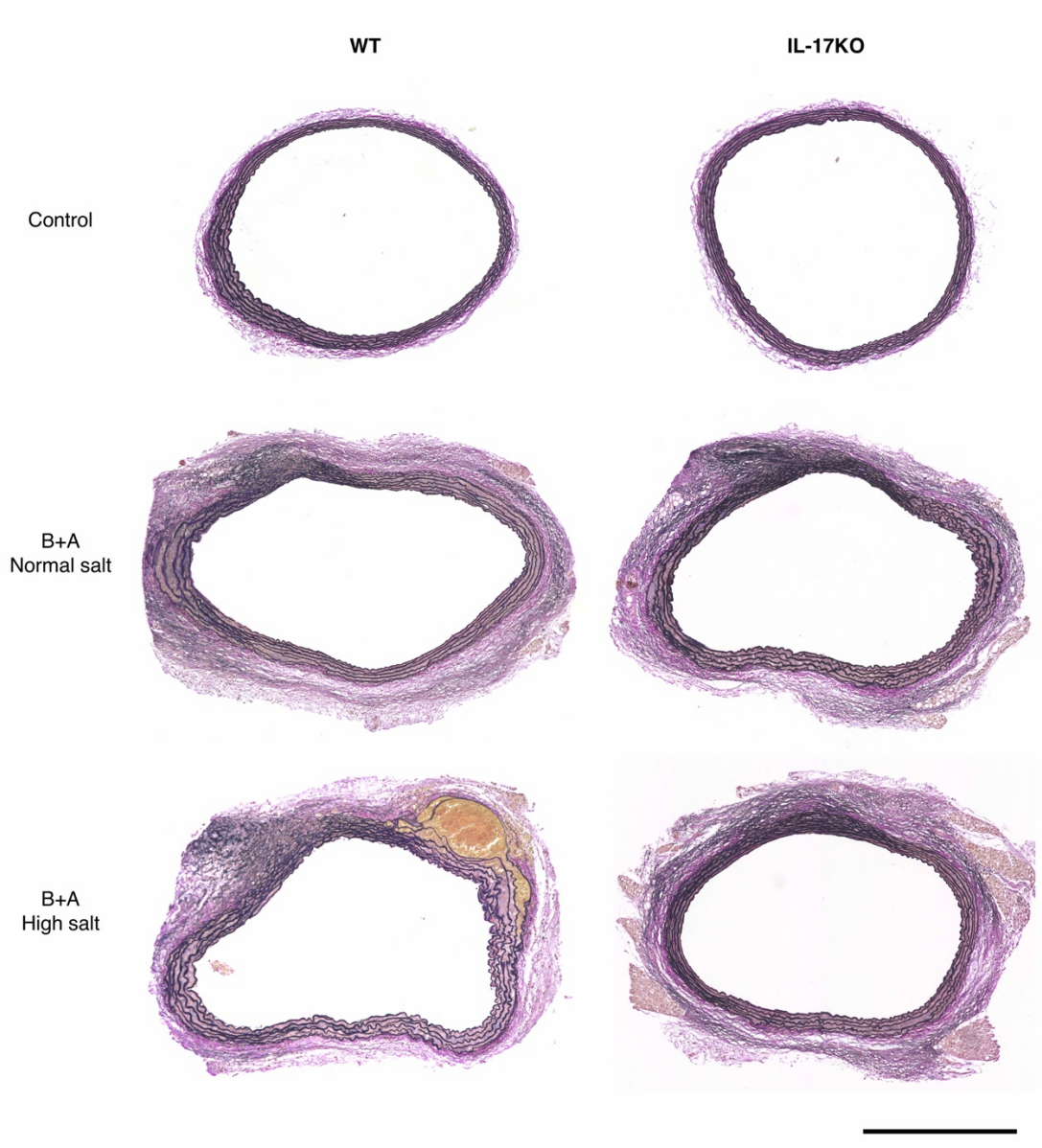

Supplemental Figure SVII. Histology of the AD model induced by BAPN+AngII
Representative histochemical analysis with hematoxylin–eosin (HE) and Elastica van Gieson (EVG) stains are shown for aortic samples from WT and IL-17KO mice with or without BAPN+AngII (B+A) and high salt challenge. Scale bar = 500 μm.

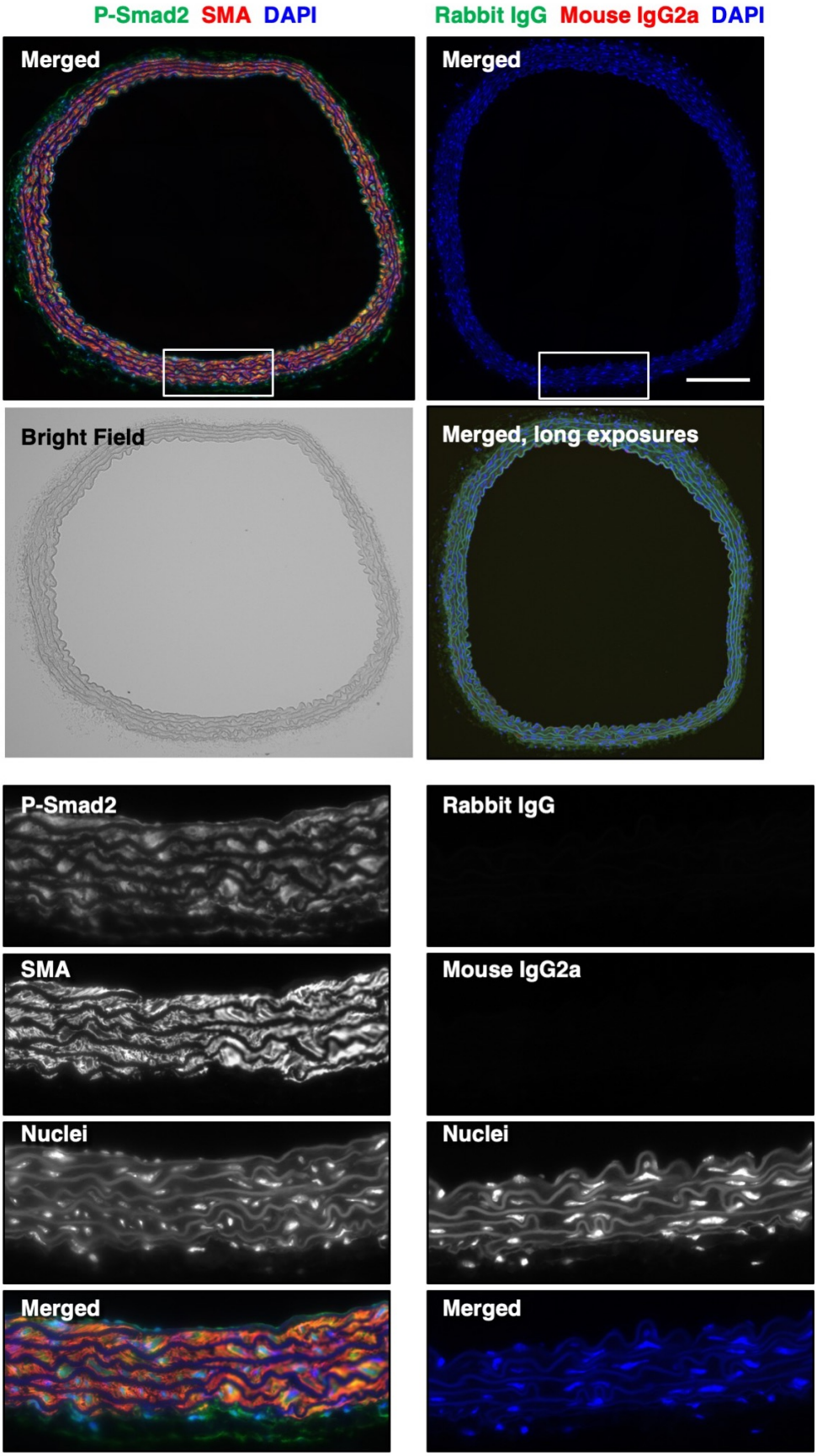
P-Smad2 SMA DAPI
Rabbit IgG Mouse IgG2a DAPI
Merged
Merged
Bright Field
Merged, long exposures
P-Smad2
Rabbit IgG
SMA
Mouse IgG2a
Nuclei
Nuclei
Merged
Merged

Supplemental Figure SVIII. Immunofluorescent staining of P-Smad2 and SMA. Left, Representative images are shown for immunofluorescent staining of phospho-Smad2 (P-Smad2), smooth muscle α-actin (SMA), and nuclei (by DAPI) in aortas. Right, Images of the negative control in which the sample was processed with isotype control antibodies corresponding to P-Smad (rabbit IgG) and SMA (mouse IgG2a) antibodies. The bottom panels show the enlarged images for the area indicated by the rectangles in the top panels. The short exposure of the aortic tissue treated with the isotype control antibodies exibits only DAPI fluorescence, and the long exposure image exhibits DAPI fluorescence and autofluorescence of elastic lamellae, demonstrating the specificity of P-Smad2 and SMA antibodies. Scale bar = 200 μm.

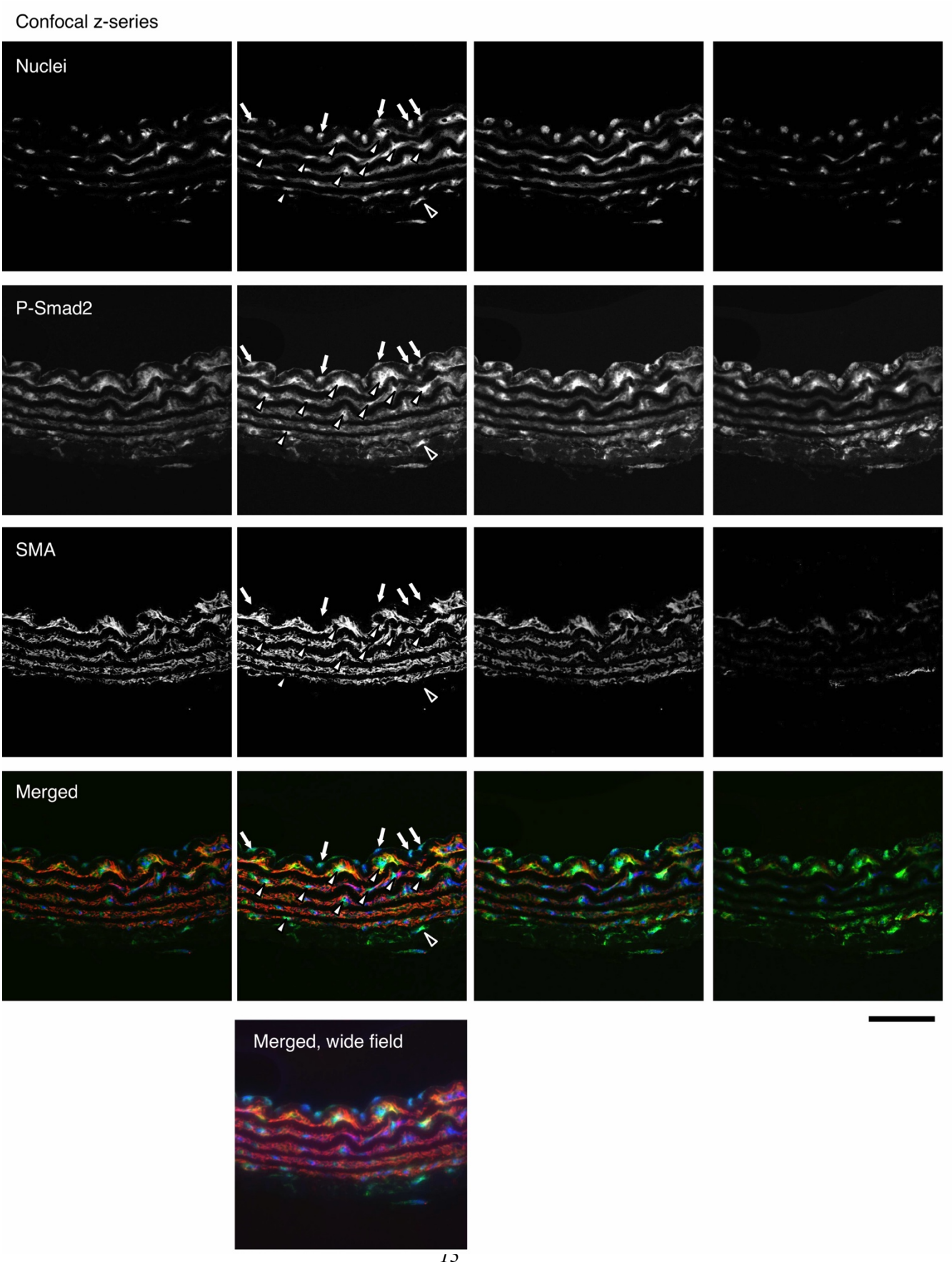
Confocal z-series
Nuclei
P-Smad2
SMA
Merged
Merged, wide field

Supplemental Figure SIX. Confocal imaging of P-Smad2 and SMA.

Representative z-series images of optical sectioning by the laser confocal microscope for immunofluorescence staining of P-Smad2, smooth muscle α-actin (SMA), and nuclei. In merged images, nuclei, P-Smad2, and SMA are pseudo-colored blue, green, and red, respectively. White arrowheads, black arrowheads, and white arrows indicate SMA-positive cells, SMA-negative adventitial cells, and SMA-negative endothelial cells, respectively. An image from the conventional wide-field fluorescence microscope is also shown for the corresponding field. Scale bar = 50 μm. The z-series images show that the 5-μm sections contain a single layer of nuclei, and part of the P-Smad2-positive nuclei were surrounded by SMA, indicating that these cells were P-Smad2-positive smooth muscle cells.

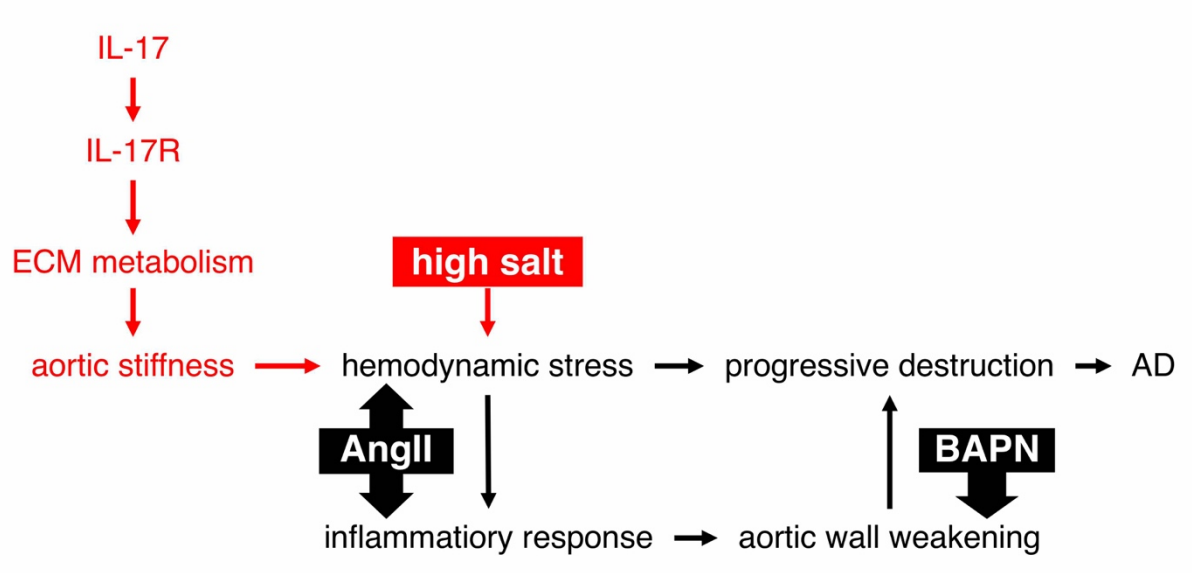

Supplemental Figure SX. Proposed mechanism for high salt and IL-17-dependent worsening of AD.

The AD model was created by continuous infusion of angiotensin II, which induces an inflammatory response and hemodynamic stress in aortic walls, and BAPN, which weakens aortic walls. IL-17 modulates ECM metabolism, causing aortic stiffness. High salt challenge augments the hemodynamic stress on stiff aorta, leading to a worsening of AD.

LEGENDS FOR SUPPLEMENTAL TABLES

Supplemental Table S1. Functional annotation of genes induced by BAPN+AngII.
Genes significantly induced by BAPN+AngII challenge (fold changes > 2.0 and $p < 0.05$) underwent functional annotation analysis using DAVID. The results correspond to the hierarchical clustering analysis and heatmap representation in Figure 1C.

Supplemental Table S2. Functional annotation of genes suppressed by BAPN+AngII.
Genes significantly suppressed by BAPN+AngII challenge (fold changes < 0.5 and $p < 0.05$) underwent functional annotation analysis using DAVID. The results correspond to the hierarchical clustering analysis and heatmap representation in Figure 1C.

Supplemental Table S3. Transcriptome of ECM-related genes.
The results of the transcriptome analysis are shown for genes with “extracellular matrix” in their Gene Ontology terms. The result corresponds to the hierarchical clustering analysis and heatmap representation in Figure 5.